Plasmonics (2010) 5:149–159
DOI 10.1007/s11468-010-9129-8

Surface Plasmon Resonance and Enhanced Fluorescence Application of Single-step Synthesized Elliptical Nano Gold-embedded Antimony Glass Dichroic Nanocomposites

Tirtha Som · Basudeb Karmakar

Received: 3 July 2009 / Accepted: 1 February 2010 / Published online: 25 February 2010

Abstract A novel series of elliptical gold (Au^0) nanoparticles (18–40 nm) embedded antimony glass (K_2O-B_2O_3-Sb_2O_3) dichroic nanocomposites have been synthesized by a single-step melt-quench in-situ thermochemical reduction technique. X-ray and selected area electron diffractions manifest growth of Au^0 nanoparticles along the (111) and (200) crystallographic planes. The transmission electron microscopic image reveals elliptical Au^0 nanoparticles having an aspect ratio varying in the range 1.2–2.1. The dichroic behavior of the nanocomposites arises due to elliptical shape of the Au^0 nanoparticles. These nanocomposites show strong surface plasmon resonance (SPR) band of Au nanoparticles in the range 610–681 nm and it exhibit red-shifts with increasing Au concentration. They, when co-doped with Sm_2O_3 and excited at 949 nm, exhibit about sevenfold enhancement of the upconverted red emission transition of $^4G_{5/2} \rightarrow {}^6H_{9/2}$ at 636 nm due to local electric field enhancement effect of Au^0 nanoparticles induced by its SPR. These nanocomposites are the promising materials for laser, display, and various nanophotonic applications.

Keywords Surface plasmon resonance · Elliptical gold nanoparticles · Antimony glass nanocomposites · Metal-enhanced fluorescence

T. Som · B. Karmakar (✉)
Glass Technology Laboratory, Glass Division,
Central Glass and Ceramic Research Institute
(Council of Scientific and Industrial Research),
196 Raja S. C. Mullick Road,
Kolkata 700 032, India
e-mail: basudebk@cgcri.res.in

Introduction

Metallic nanostructures have been a subject of considerable interest in recent years because they are endowed with unique optical properties and functionalities contrast to their bulk counterparts [1, 2]. The optical science of plasmonic metallic nanostructures and their potential application have rapidly emerged into an important field called plasmonics [3, 4]. The physical basis of absorption of light by metallic nanoparticles is the coherent oscillation of the conduction band electrons upon interacting with the electromagnetic radiation [5]. This phenomenon termed as "surface palsmon resonance (SPR)," is localized near the boundary between the metal nanostructures and the surrounding (dielectric) matrix and produces an enhanced electric field at the interface [6, 7]. Some of the most prevalent application of nanostructured materials which utilizes the evanescent field at the surface are surface-enhanced Raman scattering, surface-enhanced fluorescence, surface plasmon resonance imaging and spectroscopy, surface-enhanced second harmonic generation, and photothermal imaging and therapy [1, 8, 9]. Realization of the above phenomena in active and real functional devices with plasmonic nanoparticles requires a fundamental control of their synthesis/insertion within solid-state environment. Consequently metal-dielectric (here glass) composites are receiving significant exposures [9–20]. Such metal-dielectric (glass) nanocomposites also find other ubiquitous applications like solid-state lasers, sensors, memory devices, dichroic polarizers, colored glasses, ophthalmic lenses, display devices, and opto-electronic materials due to non-linear optical properties [9–20].

Glasses present some superior inherent advantages over other dielectrics, like high transparency, mechanical strength, ease of fabrication in desirable shapes and sizes,

and absence of metal-ligand interactions (high energy stretching vibrations). These make them promising encapsulating hosts for both metal nanoclusters and rare-earth (RE) ions. Consequently, an emerging application of metal-glass nanocomposites in the field of plasmonics is their development as substrates (hosts) capable of providing large electromagnetic enhancements or "hot spots" formation for nanometal-enhanced luminescence of rare-earth ions [16, 21–23]. Plasmonic metal nanoparticles absorb more light than indicated by their geometrical cross section [1]. These nanoparticles act as "photon catchers," concentrating a significant quantity of electromagnetic energy into a very small region around them. Thus they can improve many applications (such as fluorescence enhancement) that can benefit from this kind of light harnessing or field enhancement. The plasmon-induced/-enhanced luminescence observed in monometallic:rare-earth (RE) hybrid composites have currently captured exponential attention due to their relevance as color displays, optical amplifiers, as well as optical sensors [21–23].

Preparation of nano metal-doped conventional glass systems are not simple and demand multi-step techniques like sol-gel process, metal-dielectric co-sputtering deposition, direct metal-ion implantation, pulsed laser deposition, ion-exchange of thin plates, followed by long time heat treatment at high temperatures in reducing (hydrogen) atmosphere or UV-light/X-ray/^{60}Co γ-radiation or laser/synchrotron irradiation [9–19]. These customary techniques are generally used to incorporate thin layers of spherical or quasi-spherical metal nanoclusters within high phonon (resonance vibration energy of the matrix) matrices like silicate, borate, and phosphate glasses. It is known that the maximum local field enhancement occurs at mid-point between two interacting spherical metallic particles. However, the field enhancement for a nonspherical nanoparticle is considerably greater than that of a spherical particle of comparable size [3, 24]. Irradiation of spherical particles with ultrashort laser pulses leads to the formation of ellipsoidal particles [19, 20]. Formation of elliptical nanoparticles is an essential requirement to develop dichroic glasses [19, 20]. Therefore, simplification of preparation techniques leading to the fabrication of new bulk dielectric (glass) matrices incorporating metal nanoparticles in high yield with significant applications in the area of plasmonics is of paramount importance.

Heavy metal oxide (HMO)-based glass hosts with low phonon energy are more encouraging than silicate, borate, and phosphate systems because they provide better upconversion efficiency of RE ions by reducing their multiphonon relaxation rate. In addition HMO glasses also possess high refractive index, large transmission windows, and large non-linear optical properties [25]. Consequently, the synthesis of new HMO glass compositions embedding metal nanoparticles and RE ions have been the focus of much attention in recent years due to the potentially promising applications [21–23].

Among the HMO glasses, we have directed our attention primarily to Sb_2O_3-based systems for photonic (plasmonics), particularly surface-plasmon-enhanced luminescence applications due to the two unique properties of Sb_2O_3. Firstly, Sb_2O_3 glasses have low phonon energy (602 cm^{-1}) compared to conventional glass systems [22, 23, 25–27]. Secondly, it is a mild reducing agent (Sb^{5+}/Sb^{3+}, E^0=0.649 V) [28] and consequently it exhibits selective reduction property which can be utilized to synthesize nano metal-embedded and nano metal:RE co-embedded (hybrid) nanocomposites [22, 23, 27]. Here we have demonstrated how these two properties of antimony glasses make them distinctive for photonic application in the entire glass family. It must also be accentuated that the area of nano metals-doped and RE-doped Sb_2O_3-based glasses and nanocomposites have remained widely unexploited because of their difficulties in preparation particularly in the bulk monolithic form which is very much essential for practical photonic application. Inadequate literature reports available on synthesis of high Sb_2O_3 containing glasses show they all yielded in very tiny pieces or pulverized form [29, 30]. This is because the low field strength (0.73) of Sb^{3+} makes it a poor glass former [25]. Also intense vaporization of Sb_2O_3 during melting and high devitrification during casting has made their synthesis extremely difficult. We are the first to report the novel properties of metal-antimony glass nanocomposites.

By appropriate selection of composition, melting temperature, time, and casting mold, we demonstrate in this study a simple single-step reproducible melt-quench technique to synthesize monolithic dichroic nano Au-embedded antimony glass nanocomposites. The resultant Au-embedded nanocomposites are characterized by UV-Visible absorption spectroscopy, X-ray diffraction (XRD) analysis, transmission electron microscopy (TEM), and selected area electron diffraction (SAED) analysis. To explore the photonic (plasmonic) application, we have used the same single-step methodology to prepare Sm^{3+}:Au^0 co-embedded hybrid antimony glass nanocomposites. All the results are explained with the help of electrodynamics theory. The effect of Au^0 NPs on the upconversion fluorescence emission (visible) of Sm^{3+} under photoexcitation of longer wavelength (NIR) radiation (949 nm) is also investigated.

Experimental

The raw materials were potassium metaborate, $KBO_2 \cdot \times H_2O$ (15.7% H_2O, Johnson Matthey), antimony(III) oxide, Sb_2O_3 (GR, 99%, Loba Chemie), and chloroauric acid, $HAuCl_4 \cdot \times$

H_2O (49% Au, Loba Chemie), and samarium(III) oxide, Sm_2O_3 (99.99%, Indian Rare Earth). All the raw materials were mixed thoroughly in isopropyl alcohol medium in an agate mortar followed by drying. The base glass of composition (mol%) $15K_2O$-$15B_2O_3$-$70Sb_2O_3$ (KBS) was prepared in a 20-g melt size using above mixed raw materials in a high purity silica crucible at 900 °C in air for 10 min in a raising hearth electric furnace followed by intermittent stirring of 0.5 min. The molten glass was cast into a carbon plate and annealed at 260 °C for 3 h. The Au^0-doped nanocomposites were prepared in a similar technique using respective dopant concentrations (in excess) as shown in Table 1. To study the photonic application, a Sm_2O_3 and Au^0 co-doped (0.3 and 0.03 wt.%, respectively) nanocomposite was synthesized similarly. The melting and annealing times were kept constant for all the samples. Samples of about 2.0±0.01 mm thickness for optical measurements were prepared by cutting, grinding, and polishing with cerium oxide.

The density was measured by the Archimedes method using toluene as immersion liquid with an error of ±0.7%. Density of toluene at the experimental temperature was found to be 0.861 g cm^{-3}. The X-ray diffraction patterns of the bulk samples were recorded in an X'pert Pro MPD diffractometer (PANalytical) operating at 40 kV and 30 mA using Ni-filtered Cukα radiation with the X'celerator with step size 0.05º (2θ) step time 0.5 s, from 10º to 80º. TEM was done using a Jeol (model JEM 2010) operating at an accelerating voltage of 200 kV. The UV-Vis transmission spectra were obtained with a double-beam spectrophotometer (Lambda 20, Perkin-Elmer). The uncertainty of the band position is ±0.1 nm. Fluorescence spectra were measured, at the error of ±0.2 nm, with a fluorescence spectrophotometer (Spex, Fluorolog 2, Perkin-Elmer) in which a xenon lamp is attached as an excitation source and a photomultiplier tube as a detector. The excitation slit (1.25 mm) and emission slit (0.5 mm) was kept same for all the samples so that the excitation intensity was as nearly as possible the same for all the samples. All the measurements were carried out at room temperature. The enhancement of luminescence was found to be reproducible for all the samples.

Results and discussion

The composition of base glass, nanostructured composite glasses (NCGs), and some of their properties are listed in Table 1. All nanocomposites were obtained in the monolithic form. The density of the nanocomposites increases linearly with increase in Au concentration. The base glass (B) is pale yellow due to transition between HOMO (Sb 5 s+O 2pπ) and LUMO (Sb 5p) [25, 26]. It was observed that all the nanocomposites were dichroic, i.e., they transmitted the blue color (Fig. 1a) and reflected the brown to reddish-brown (Fig. 1b) light. The intensity of the reflected brown color increases with increase in Au^0 concentration.

Figure 2 displays the XRD spectra of the synthesized nanocomposites. The broad XRD band, particularly the hump between 25º to 35º of base glass (B), (Fig. 2, curve a) indicates the amorphous nature of the synthesized base glass due to presence of uncrystallized Sb_2O_3 or other constituents. The sharp peak at 2θ=38.4021º (d=2.34216 Å) and 44.1634º (d=2.04906 Å; curves b–e) is assigned as (111) and (200) diffractions of fcc Au^0 nanoparticles (JCPDS, card file no. 4-0784) embedded within the antimony borate glass matrix (Fig. 2, curves b–g). However, the XRD diffraction peaks are fairly weak because the concentration of the nano metal-embedded within bulk amorphous dielectric (KBS glass) matrix is very low. The XRD spectrum manifests the reduction of Au^{3+} to Au^0 by the reducing glass matrix component Sb_2O_3 since no other external reducing agent is present. As the size of the nanocrystals decreases, the peak line width in the XRD spectra is broadened due to loss of long-range order relative to the bulk. This XRD line width

Table 1 Composition and some properties of Au-antimony glass dichroic nanocomposites

Sample identity no.	Concentration of Au (wt.%)[a]	Density (g.cm^{-3})	Color of transmitted light	Color of reflected light	SPR band position (±1, nm)	Particle size of Au from Eq.1 (±1, nm)
B	-	4.556	Yellow	Yellow		
NCG1	0.001	4.557	Blue	Brown	610	18
NCG2	0.003	4.560	Blue	Brown	610	20
NCG3	0.03	4.575	Blue	Brown	612	24
NCG4	0.1	4.583	Blue	Brown	680	30
NCG5	0.3	4.587	Blue	Reddish- brown	681	36
NCG6	0.5	4.590	Blue	Reddish-brown	681	40

[a] Base glass (B) composition (mol%): $15K_2O$-$15B_2O3$-$70Sb_2O_3$. All Au concentrations are in excess

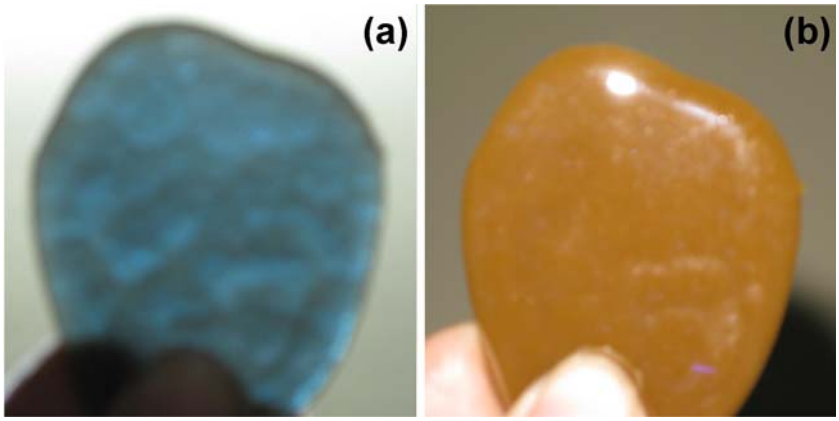

Fig. 1 (*Color online*) Photograph showing dichroic behavior of Au-antimony glass nanocomposites: (**a**) *blue* in transmitted light and (**b**) *brown* in reflected light

can be used to estimate the size of the particle by using the Debye–Scherrer formula as [1]:

$$d = \frac{0.9\lambda}{\beta \cos 2\theta} \quad (1)$$

where d is the nanocrystal diameter, λ is the wavelength of X-ray radiation, β is the full-width half-maximum (FWHM) of the peak in radians, and 2θ is the Bragg angle. The calculated average diameter of the Au^0 nanocrystallites, as calculated by using Debye–Scherrer's formula (Eq. 1), is found to be varied in the range 18–40 (±1) nm. They are listed in Table 1.

The sharp peaks at 2θ=19.5366° (d=4.54013 Å), 25.5436° (d=3.48443 Å), and 28.5159º (d=3.12764 Å) are corresponds to (110), (111), and (121) diffractions of valentinite form of Sb_2O_3 crystals (JCPDS, card file no. 11-689) created within the antimony borate glass matrix due

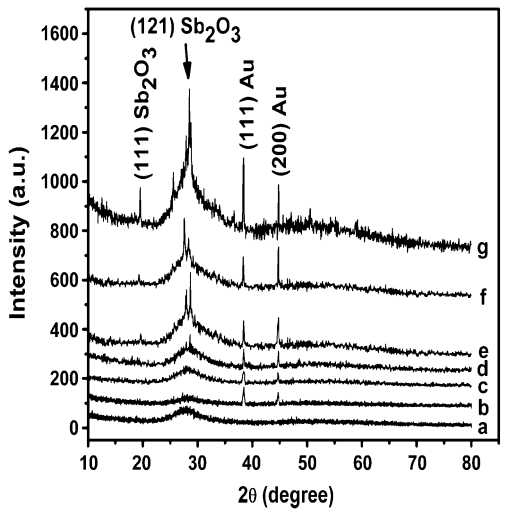

Fig. 2 XRD pattern of (**a**) base glass B showing amorphous nature of the glass and nanocomposites (**b**) NCG1, (**c**) NCG2, (**d**) NCG3, (**e**) NCG4, (**f**) NCG5, and (**g**) NCG6 showing nano Au^0 and crystallized valentinite type phases of Sb_2O_3 (for composition see Table 1; *a.u.* stands for arbitrary unit)

to crystallization of some Sb_2O_3 of the matrix by very high concentrations of Au [31]. Au metallic nuclei formed in this manner precipitated throughout the body of the glass act as heterogeneous nuclei for crystallization of Sb_2O_3 in K_2O-B_2O_3-Sb_2O_3 system [31]. Large difference in field strength (F) between Sb^{3+} (0.73) and B^{3+} (F=1.63) [25] and the presence of Au^0 have encouraged in phase separation and thereby the precipitation of nano dimension antimony oxide crystals.

The TEM image (Fig. 3a) of the Au^0 NPs (nanocomposites NCG-2) shows nanoparticles majority of which have elliptical. The major axis (diameter) of the NPs ranges from 5 to 18 nm (±3%) while minor axis varies between 4 and 12 nm (±3%). The average aspect ratio of the elliptical Au^0 NPs is found to be varied in the range 1.2–2.1. The dichroic behavior of the nanocomposites arises due to the elliptical shape of the Au^0 NPs. Here the mechanism of deformation or the formation of elliptical nanoparticles by the simple single-step melt-quench process is probably due to the influence of the high viscosity of the molten Sb_2O_3-based matrix on the Au^0 colloids. It has been documented in literature that prolate ellipsoid Ag NPs having an aspect ratio around 1.2 exhibits the phenomenon of dichroism [19, 20] due to the difference in polarizations along the major (longitudinal) and minor (transverse) axes of a polarizable ellipsoidal nanoparticle in presence of electromagnetic wave. It has also been observed that for such elliptical (elongated) Ag NPs the SPR peak obtained from the interaction of transversely polarized light is different from the SPR peak position acquired in presence of longitudinally polarized light corresponding to transverse and longitudinal electron oscillations (with respect to the particle principal axis), respectively [19, 20, 32]. Since longitudinal and transverse localized plasmon resonances of elliptical metal nanoparticles are basically independent of each other, that is, it is possible to selectively excite them by using light with oscillating electric field parallel and perpendicular to the major axis of the ellipsoids (polarization-dependent optical response),

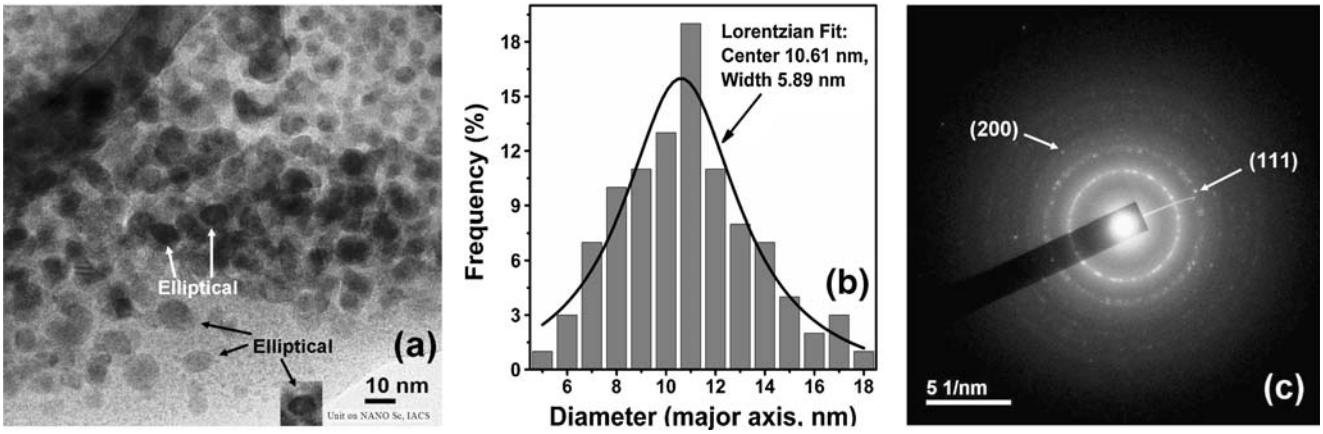

Fig. 3 (**a**) TEM image of nanocomposite NCG2 (*inset* shows elliptical Au nanoparticle). (**b**) Histogram of TEM image (**a**). (**c**) The SAED pattern of a Au nanoparticles (for composition see Table 1)

consequently such dichroic nanocomposites are therefore possible candidates for displays or encoding security systems [33] and for making dichroic glass polarizers [19]. From the TEM observation (Fig. 3a), the frequency of nanoparticles versus particle diameter (major axis) surveyed from the grain boundaries for the area displayed in the image has been plotted in Fig. 3b using Origin 7.0 Software. The particle distribution gives a better fit for the Lorentzian function and the average particle size is about 11 nm. The difference between the average particle obtained from the TEM image (histogram) and the XRD spectra arises due to the fact that the XRD spectra gives the average of the total particles present while the TEM image shows particles only in a particular section. The SAED image (Fig. 3c) shows the presence of (111) and (200) crystallographic planes of Au^0 and correlates well with XRD patterns.

The UV-Visible absorption spectrum is the most important tool to detect the formation of noble metal NPs and SPR bands. The UV-Vis-NIR absorption spectrum of the undoped glass (shows absence of any features indicating the base glass matrix is transparent in the spectral region of interest to this study (Fig. 4, curve a). The absorption spectra of the Au-doped NCGs (Fig. 4, curves b–g) display well-defined broad plasmon (SPR) absorption bands (610–681 nm) characteristic of nano-sized Au^0. Typically the SPR for nano Au in sodaline silicate glass (refractive index ~ 1.5) appear around 520 nm for near-spherical nanoparticles. But here in KBS antimony glass the maxima of the plasmon peaks (λ_{max}), listed in Table 1, experience a distinctive red-shift towards higher wavelength (from 610 to 681 nm) with increase in Au^0 concentration (from 0.001 to 0.3 wt.%). At higher concentration the SPR band gradually broadened and their tails have extended up to 1,100 nm. This type of complex system where a high refractive index dielectric matrix encompasses closely spaced elliptical nanoparticles having electromagnetic coupling, the need arises for theory that can describe the electrodynamics of such nanoparticles [4, 11, 34, 35].

From the electromagnetic viewpoint, nano metals are plasmas, comprising of fixed, positive ion cores and oscillating conduction electrons whose resonant frequency arises from the restoring force that the altered charge distribution exerts on the mobile charges when they are displaced from equilibrium [1, 8]. This is schematically pictured for an elliptical particle in Fig. 5 which results in SPR absorption. Because gold or silver particles have essentially "free," that is, very weakly bound conduction electrons, oscillations of which lie low enough in energy to be in the visible spectral region [1, 34–36].

For nanoparticles very small compared to the wavelength λ of incident light ($\lambda >> d$, for gold nanoparticles $d<25$ nm) only the dipole absorption of the Mie equation contributes to

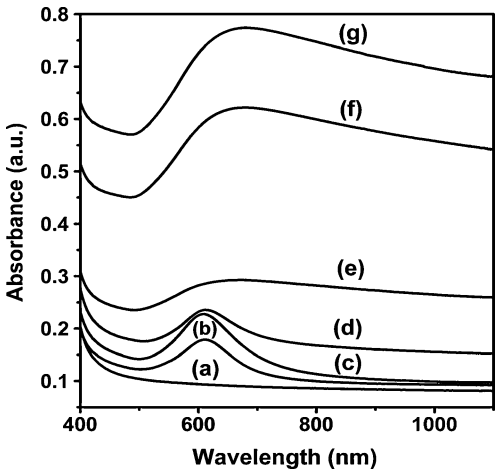

Fig. 4 UV-Vis absorption spectra of (**a**) based glass B and nanocomposites (**b**) NCG1, (**c**) NCG2, (**d**) NCG3, (**e**) NCG4, (**f**) NCG5, and (**g**) NCG6 (for composition see Table 1, a.u. is absorbance unit)

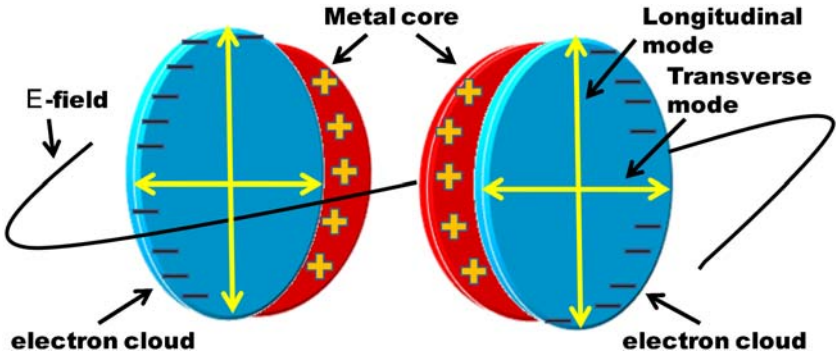

Fig. 5 (*Color online*) Schematic illustration of plasmon resonance in elliptical gold nanoparticle

the extinction cross section of the nanoparticles and the SPR absorption is produced at optical frequency ω at which the resonance condition $\varepsilon_r=-2\varepsilon_m$ is fulfilled. Here ε_m is the dielectric constant of the surrounding medium and ε_r is the real part of the material (Au) dielectric function dependent on the angular frequency of light. The SPR band should be independent of size within the dipole approximation. But practically the plasmon band width increases with decrease in particle size for particles smaller than 20 nm. The size dependence of the dielectric constant of the metal is introduced as the diameter of the particle becomes smaller than the mean free path of the conduction electrons. This is referred as "intrinsic size effect" [3, 34, 35].

For noble metal nanoparticles like gold, there are two types of contributions to the dielectric function of the metal. First contribution is from the inner d-electrons which give rise to interband transition from the inner d-orbitals to the outer conduction band (interband term $\varepsilon_{IB}(\omega)$) while the second contribution is from the free conduction band electrons (Drude term $\varepsilon_D(\omega)$) which is described by the Drude free electron model as [3, 18, 34, 35]:

Thus for extremely small particles (<25 nm for gold), the shift of the SPR band peak position is rather small (610–612 nm, see Table 1). However, a broadening of the peak is expected. This is observed practically for nanocomposites NCG1–NCG3 (see Fig. 4, curves b–d).

For nanoparticles of larger dimension (d>25 nm for gold nanoparticles), significant contributions are made by higher-order (quadrupolar) charge cloud distortion of conduction electrons as well as scattering [35]. These contributions induce drastic red-shift (from 610 to 681 nm, see Table 1) of the SPR peak with the increase in particle diameter d (30–40 nm, see Table 1) and the bandwidth also increases. This is practically observed for nanocomposites NCG4–NCG6 (see Fig. 4, curves e–g). This effect for larger size particles is called "extrinsic size effect" [3, 34, 35]. The broadening of the plasmon band is then usually attributed to retardation effects [35].

As evident from the resonance condition, the shape and position of the SPR band is also influenced by the dielectric constant of the surrounding. This constitutes the basis of "immersion spectroscopy" [3]. When $\omega_p>>\gamma$, the SPR absorption maxima λ_{max}, is susceptible to the changes of refractive index, n_m of the surrounding medium as [36]:

$$\lambda_{max} = \lambda_p\left(2n_m^2+1\right)^{1/2} \tag{2}$$

where $n_m=(\varepsilon_m)^{1/2}$. Thus, the SPR peak exhibits a red-shift with increase in medium refractive index [3, 36]. Our KBS antimony glass having a refractive index about 1.947, radically red-shifts the plasmon peak to around 610 nm. Beside increase in ε_m is also expected to result an increase in plasmon band intensity and band width [3, 36]

In addition, the SPR peak of nonspherical metal NPs is generally red-shifted compared to spherical ones [3]. Elongated particles may show two maxima if the aspect ratio is ≥4. The longitudinal resonance signal in case of gold, with an aspect ratio of 4, shifts from 520 to 770 nm [37]. Within the dipole approximation, the Gans theory [38], which is the extended form of Mie theory, is applicable for small ellipsoidal (prolate and oblate) particles. For ellipsoidal particles, the plasmon resonance may split into two distinct modes depending on its aspect ratio. Such splitting is the result of surface curvature which decides the restoring force or depolarization effect that acts on the resonating conduction band electrons. Consequently, the extinction cross section, C_{ext}, of ellipsoidal particle is directly proportional to its imaginary part of polarizability, α_{ED} as [38, 39]:

$$C_{ext} = 2\pi n_h \mathrm{I}(\alpha_{ED})/\lambda \tag{3}$$

where

$$\alpha_{ED} = V\varepsilon_m \frac{\varepsilon_{Au}-\varepsilon_m}{\varepsilon_m + L_j(\varepsilon_{Au}-\varepsilon_m)} \tag{4}$$

$j=x, y, z$ denotes the principal axes of the ellipsoid, $V=(4R_xR_yR_z)/3$ and L_j are depolarization factors given by [39]:

$$L_j = \frac{R_xR_yR_z}{2}\int_0^{\alpha} \frac{\mathrm{ds}}{\left(\mathrm{s}+R_j^2\right)\sqrt{\left(\mathrm{s}+R_x^2\right)\left(\mathrm{s}+R_y^2\right)\left(\mathrm{s}+R_z^2\right)}} \tag{5}$$

where the condition $L_x+L_y+L_z=1$ is fulfilled, and R_j are the corresponding lengths of the half axes of the ellipsoid along

the x, y, and z-axes. The depolarization factor for the respective axis is given by [38]:

$$L_x = \left[\left(1-e^2\right)/e^2\right]\left[-1+(1/2e)\ln(1+e)/(1-e)\right] \quad (6)$$

$$L_{y,z} = (1-L_x)/2 \quad (7)$$

where $e=[1-(b/a)^2]^{1/2}$ is the eccentricity of the ellipsoid. For the degenerate case of a sphere $e=0$, or $R_x=R_y=R_z$, $Lj=1/3$. Under these conditions, the birefringence disappears. The implied meaning of Eq. (6) is very clear. Oriented ellipsoids exhibit strong polarization-dependent optical spectra. Simply, nanocomposites exhibits dichroic behavior (see Fig. 1), that is, one color in the transmitted light and a different color in the reflected light [19]. Thus for $R_x/R_y=1$, the Gans theory become Mie theory. The denominator of Eq. 4 is resonant at the surface plasmon resonance. Consequently, the new SPR position is modified as:

$$\varepsilon_{\mathrm{Au}} = \left(-1/L_j+1\right)\varepsilon_{\mathrm{m}}, \quad (8)$$

Hence by changing the shape the SPR can be tuned across a wide spectroscopic region. It is thus established SPR is intimately controlled by the nanoparticle size, shape, refractive index of the dielectric host (here glass), and other proximal NPs.

Plasmonics can be used to modify the radiative decay properties of RE ions or fluorophore molecules. By using metal nanoparticles of different shapes, sizes, and its associated local field and by varying the metal-RE ions distance, an enhanced quantum yield or quenched fluorescence can be obtained. This approach is referred to as "radiative decay engineering" [3, 40].

The plasmonic (photonic) efficiency of these co-doped composites and the flexibility and advantage of the present versatile method and is demonstrated by synthesizing RE (here Sm^{3+}):Au^0 co-doped antimony based hybrid nanocomposite by analogous single-step route. A probable mechanism can be deduced using reduction potential values (Sm^{3+}/Sm^0, $E^0=-2.304$ V and $Sb^{5+}/Sb^{3+}=0.649$ V), as described later [28]. The absorption spectrum with the details of peak positions (energy levels) of 0.3 wt.% (in excess) Sm_2O_3-doped base glass (B) has been illustrated in our earlier work [26]. The Sm^{3+}-doped antimony glass displays an absorption band at 949 nm. So, under 949 nm excitation radiation the processes of ground state absorption (GSA) and subsequent excited state absorption (ESA), energy transfer (ET), and cooperative energy transfer (CET) take place between two neighboring Sm^{3+} ions as:

$$^6H_{5/2} \rightarrow {}^6F_{11/2}(\mathrm{GSA}) \rightarrow {}^4I_{11/2}[\mathrm{ESA}]$$

$$\left({}^6F_{11/2}, {}^6F_{11/2}\right) \rightarrow \left({}^4G_{5/2}, {}^6H_{11/2}\right)[\mathrm{ET}]$$

$$\left({}^6F_{11/2}, {}^6F_{11/2}\right) \rightarrow \left({}^4F_{3/2}, {}^6H_{9/2}\right)[\mathrm{ET}]$$

$$\left({}^4I_{9/2}, {}^6F_{7/2}\right) \rightarrow \left({}^4G_{5/2}, {}^6F_{11/2}\right)[\mathrm{CET}]$$

The non-radiative relaxation (NR) processes from higher levels results in the population of the $^4G_{5/2}$ metastable radiative storage level. Consequently, the Sm^{3+}-doped glass shows upconverted emission bands observed at 566 (green, weak), 602 (orange, weak), 636 (red, very strong), and 649 (red, very weak) nm due to $^4G_{5/2} \rightarrow {}^6H_{5/2}$ ($\Delta J=0$, zero–zero band, forbidden transition), $^4G_{5/2} \rightarrow {}^6H_{7/2}$ ($\Delta J=1$, magnetic dipole transition), $^4G_{5/2} \rightarrow {}^6H_{9/2}$ ($\Delta J=2$, electric dipole transition), and $^4G_{5/2} \rightarrow {}^6H_{11/2}$ ($\Delta J=3$, forbidden transition), respectively [26]. These are shown in Fig. 6 (curve a) and interpreted with the help of partial energy level diagram of Sm^{3+} ion in KBS glass (Fig. 7).

The electric dipole allowed $^4G_{5/2} \rightarrow {}^6H_{9/2}$ transitions undergoes drastic intensity enhancement in presence of the elliptical Au NPs when photoluminescence upconversion of the Sm^{3+}:Au co-doped nanocomposites is carried out under the same excitation wavelength. It is to be noted here that different monometallic:rare-earth ions co-embedded (Sm^{3+}:Au) KBS glasses having concentrations (in wt.%) (a) $0.3Sm^{3+}$:0.003Au, (b) $0.3Sm^{3+}$:0.03Au, and (c) $0.3Sm^{3+}$:0.3Au have been examined for fluorescence enhancement. The maximum enhancement was found to be

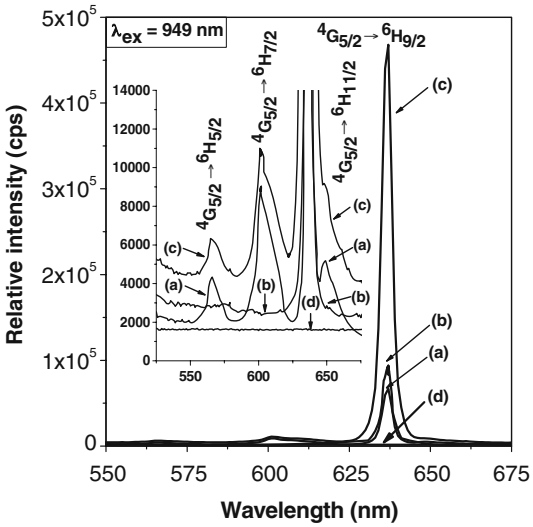

Fig. 6 Upconversion spectra of (**a**) 0.3 wt.% Sm^{3+}-doped, (**b**) 0.03 wt.% Au-doped (NCG3), (**c**) 0.3 wt.% Sm_2O_3 and 0.03 wt.% Au co-doped, and (**d**) base glass under excitation wavelength at $\lambda_{ex}=$ 949 nm. *Inset* shows the enlargement in the wavelength region 525–675 nm. The unit *cps* stands for photon counts per second

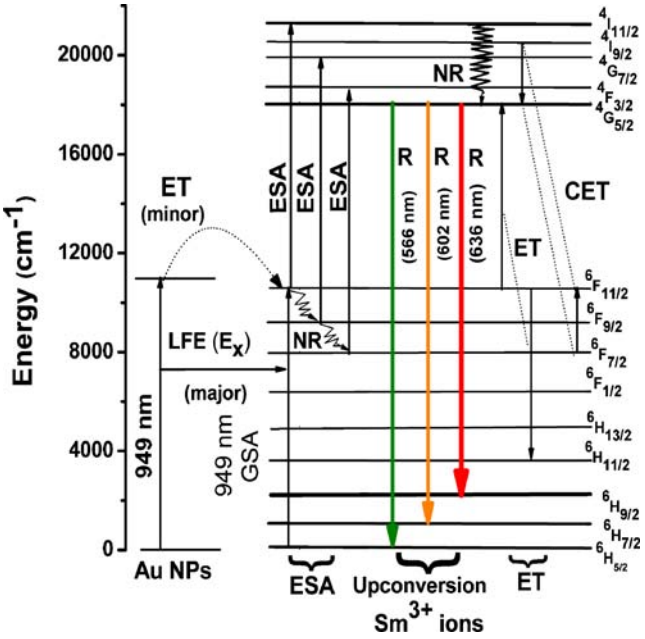

Fig. 7 (*Color online*) Partial energy level diagram of Sm^{3+} ion coembedded with Au NPs in KBS glass showing upconversion fluorescence emissions at 566, 602, and 636 nm through *GSA*, *ESA*, *ET*, and *CET* between Sm^{3+} ions. *LFE* by SPR of elliptical Au NPs and ET from Au NPs to Sm^{3+} ions in the nanocomposites are also shown (*R* and *NR* represent the radiative and non-radiative transitions, respectively)

about sevenfolds in the case of (b) $0.3Sm^{3+}$:0.03Au. So we have presented its photoluminescence upconversion spectrum in Fig. 6 (curve c) for simplicity and clear visibility eliminating the rest. Local electric field enhancement (shown as E_x in Fig. 7) and energy transfer (ET) from Au NPs to Sm^{3+} are responsible for such enhancement of fluorescence. Preserving the inherent advantages of glasses over the crystalline and polymeric competitors, these hybrid nanocomposites appear to be potential candidates for high-quality display and laser devices.

The electronic oscillations (SPR) generate surface plasmon waves (surface plasmon polaritons) that metal travel along the surface of the metal NPs (metal-dielectric interface) and concentrate light in the subwavelength structures due to the difference in relative permittivity of the metal and the surrounding glass matrix [6, 7]. Thus the nanostructures result in giant and spatially localized electric fields around Sm^{3+} ion [21–23, 41]. Metallic screening and concentration of light lead to strengthening of the local electric field, E_{loc}, around the metal nanostructures (by "Lightning Rod Effect") with respect to the incident field, E_o [7]. Thus by changing the rates of excitation and emission of RE ions, the metal NPs provide a unique opportunity to modify their fluorescence. Nano metal-enhanced fluorescence is based on the local field enhancement induced by SPR near rough metallic surfaces. Within glass matrices, the influence of metallic particles on the absorption and emission rates of RE ions is predominantly of electronic origin [41]. This can be viewed as an additional interaction due to the high field gradients in the around the metal NPs produced by plasmonic excitation of the particles at the Mie resonance frequency (SPR) [41].

A more simplistic but less accurate approach to calculate the field enhancement factor, η, (which is the ratio of the local field, E_{loc}, to the incident field, E_i) for a collection of nanoparticles of diameter d embedded in glasses and separated by the distance D, which can be deduced from the condition of the potential is expressed as [7, 22, 23]:

$$\eta = E_{loc}/E_i = (d+D)/D \tag{9}$$

Using this method [22, 23], the field enhancement factor for the 0.03 wt.% Au: 0.03 wt.% Sm^{3+} co-doped nanocomposite is found to be 4.2 at Au-Au, Sm^{3+}-Sm^{3+}, and Au-Sm^{3+} separation of 63, 27.7, and 27.6 Å, respectively.

Although it is sought to obtain localized excitation and increased quantum yield near metal NPs but in practical both enhancing and quenching of RE ions or fluorophores (as the case may be) takes place near the metal particles [42]. Literature reports that to obtain enhancement of fluorescence, the fluorophore molecule must be situated at least at a distance of 50 Å or more from the metal surface to evade quenching at shorter distances [43]. There are also distinct sectors near the surface where the enhancement effect is maximum because the local field decreases exponentially from the surface [6, 43]. In fact, the interactions between RE ions (or fluorophore molecules) with metals depend on a several factors like metal type, fluorophore type, the sizes of plasmonic metal NPs, distance between fluorophore and metal particle surface, and molecule dipole orientation versus particle surface, etc. and is fairly complex [42, 44]. For example, nano-sized metallic particles have larger field effects than continuous metallic surfaces [43]. However, it is very difficult to accurately determine the effect of each such parameter on the fluorescence properties of Sm^{3+} ions in-situ synthesized and embedded in KBS glass. The geometrical variations (e.g., elliptical, rod-shaped, triangles, etc.) of the metal NPs play a crucial role in the nanometal boosted fluorescence process. In this regard, anisotropic NPs with sharp edges are more favored contenders for nanometal-enhanced fluorescence studies [22–24]. Electromagnetic excitations induce surface charges. The local surface charge (electronic) densities are severely increased and confined near the sharp edges of anisotropic nanostructures which act as light-harvesting nano optical antennas converting visible light

into large localized electric field ("lightning-rod effect") [7]. Therefore Sm^{3+} ions trapped at the interparticle junction of anisotropic elliptical metal particles with pointed peripheries are expected to experience a greater electric field than that produced by spherical NPs.

Figure 6, curve b depicts the emission band of 0.3 wt.% Au-doped antimony nanocomposites (NCG-3). The Au NPs also emit photons at 636 nm (energy ~ 15,723 cm^{-1}) under pump excitation at 949 nm. Asymmetric Au NPs are known to exhibit photoluminescence emissions in the visible range upon excitation with NIR radiation [23]. Impregnating dielectric hosts (glass, polymers, etc.) by small semiconductors or metal clusters increases their inherent non-linear optical (NLO) response by several folds. Generally, large NLO properties are exhibited by HMO glasses containing ions of high polarizability. High Sb_2O_3 containing antimony borate glasses with a lone pair of electrons of Sb^{3+} ($5\ s^2$) are known to possess NLO (curve b) with a large value of third order non-linear susceptibility (χ^3) [29]. The calculated molar polarizability (from Lorentz–Lorenz equation) of KBS antimony glass is found to be 9.598 $Å^3$ which is considerably greater than molar polarizability of silica glass (2.965 $Å^3$). This auxiliary electric field induced by NLO glass host may also make some contribution to the allowed electric dipole $^4G_{5/2} \rightarrow {}^6H_{9/2}$ transition which results in enhancement of the red fluorescence compared to the orange and green ones in contrast to that observed in case of Sm^{3+}-doped silicate glasses [26]. The $^4G_{5/2} \rightarrow {}^6H_{9/2}$ transition, which is hypersensitive, also undergoes a forced electric dipole transition since the Sm^{3+} ions are present in asymmetric geometric environment (i.e., KBS antimony glass) of high polarizability.

Thus, when excited by NIR light, Au-doped antimony nanocomposites are found to emit visible photons due to their improved large non-linear optical properties. Formation of nanometallic elliptical nanostructures within rigid and stable glass matrix with inherent non-linear optical properties suggest the imminent employment of these photoluminescent Au-doped antimony glass nanocomposites in non-linear optics based appliances.

Therefore, another minor factor contributing to the enhanced luminescence is energy transfer from Au^0 to Sm^{3+} ($Au \rightarrow Sm^{3+}$) [21–23] (see Fig. 7). When the Sm^{3+} is present in close proximity of the metal surface, the weak photoluminescence emissions from the Au NPs is added as a second channel of excitation energy. Thus, the Au NPs increases the photonic density around the Sm^{3+} ions situated in near vicinity and thereby alter the number of photons captured by the Sm^{3+} ions. As a result of superior excitation rate the population of the excited state of the Sm^{3+} ions increases and subsequently the rate of radiative decay enhances. According to Fermi's golden rule, the transition probability W_{ij} to the ground state is given by [3, 40]:

$$W_{ij} = \frac{2\pi}{h} |M_{ij}|^2 \rho(\gamma_{ij}) \tag{10}$$

where M_{ij} is the transition dipole moment, which connects the initial (i) and the final state (j), and $\rho(\gamma_{ij})$ is the photonic mode density for the transition frequency (γ_{ij}).

These hybrid nanocomposites are budding candidates for photonic and opto-electronic applications such as in optical displays, lasers, and optical memory devices. The additional electric field induced by large non-linear optical glass host possibly makes some contribution to enhance the allowed electric dipole $^4G_{5/2} \rightarrow {}^6H_{9/2}$ transition which results in red fluorescence enhancement.

It must be emphasized that the excitation of different places of the Sm^{3+}-doped glasses and nanocomposites by the 949 nm radiation always results in the upconversion peak positions at 566, 602, 636, and 649 nm with intensity variation ±1%. This indicates the homogeneous incorporation of Sm^{3+} ions and Au in the glass and nanocomposites.

This technique offers enormous advantages in comparison to classical synthetic routes. (1) Although precise size control of the nanoparticles is ruled out but the size of the Au nanoparticles can be restricted to some extent by just controlling the $HAuCl_4 . \times H_2O$ concentration in the batch. (2) Being a simple and scalable methodology, it can be used to obtain relatively large quantities of material and bulk glasses embedded with Au nanocrystallites. (3) Since it involves in-situ chemical reduction process, the yield of Au NPs (number density) is very high. This can be envisaged from the TEM images. (4) All the Au-doped nanocomposites have brilliant blue transmission and uniform reddish-brown reflection, especially composites having higher Au concentration. Therefore, this procedure and compositions can also be considered as an appropriate alternative for the production industrial and commercial dichroic glasses at very low expenditure. (5) Such luminescent dichroic nanocomposites are promising as polarizers and high-quality display devices particularly due to the dichroic behavior as well as intense deep red (636 nm) fluorescence having a narrow FWHM. (6) Other interesting optical applications may stem from enhanced non-linearities caused by elliptical NPs with intensified local electric fields around them.

By considering the reduction potentials of the respective redox systems (E^0), that is, Sb^{5+}/Sb^{3+}, $E^0 = 0.649$ V; Au^{3+}/Au^0, $E^0 = 1.498$ V; and Sm^{3+}/Sm^0, $E^0 = -2.304$ V [28], a probable mechanism of selective chemical reduction of Au^{3+} to Au^0 by Sb^{3+} and not reduction of Sm^{3+} by Sb^{3+} can be elucidated. It should be mentioned here that the standard potential values for antimony glasses at high temperature are unavailable in the literature, so we have used here the

room temperature standard potential for simple systems at equilibrium with air. Thus, Sb^{3+} is expected to reduce Au^{3+} to Au^0, while it itself is being oxidized to Sb^{5+}. Besides Sb^{3+} has an inherent inclination to get oxidized to Sb^{5+}. Hence, the overall reaction $3Sb^{3+}+2Sm^{3+}\rightarrow 3Sb^{5+}+2Sm^0$, has an $E^0=1.05$ V which means it is a spontaneous reduction reaction having a free energy (ΔG value) around −608 kJ. The thermochemical reaction $3Sb^{3+}+2Sm^{3+}\rightarrow 3Sb^{5+}+2Sm^0$, would have an E^0 value=−6.55 V (ΔG is positive) manifesting that this reaction is non-spontaneous and thermodynamically not feasible. Besides 3+ being the highest and the most stable oxidation state of Sm and Sm^{3+}/Sm^{2+} has $E^0=-1.55$ V, Sm^{3+} would have the least tendency to undergo reduction to lower oxidation states (Sm^0 or Sm^{2+}). Thus, Sm^{3+} ion does not reduce.

We believe that this work would create new vistas for antimony glass nanocomposites and establish them as potentially advanced versatile category of photonic (plasmonic) materials.

Conclusions

A new single-step methodology (selective thermochemical reduction) has been demonstarted to generate a new series of nano Au^0-embedded bulk antimony glass dichroic nanocomposites without using any external reducing agent. The dichroism arises due to the elliptical shape of the Au nanoparticles having an aspect ratio of about 1.2–2.1, as observed in the TEM image. The XRD patterns show the presence of (111) and (200) crystallographic planes of fcc Au^0 nanoparticles. The UV-Vis absorption spectra show that the SPR peak of Au nanoparticles experience a red-shift (610–681 nm) with increasing Au concentration. The origin of SPR and its associated local field have been explained with electrodynamics theory. The superiority of the present versatile method has also been demonstrated by synthesizing Sm^{3+}:Au^0 co-doped antimony-based nanocomposite by similar single-step route and mechanism has also been discussed using reduction potential values. The photoluminescence upconversion studies of this co-embedded nanocomposite at 949 nm excitation shows that the 636 nm red emissions of Sm^{3+} ions arising due to $^4G_{5/2}\rightarrow{}^6H_{9/2}$ transition remarkably undergo about sevenfold enhancement of luminescence intensity in presence of nano Au. Such enhancement of fluorescence is attributed to the local field enhancement and energy transfer from Au^0 to Sm^{3+}. These co-doped nanocomposites are potential candidates for applications in display devices, laser sources, and other nanophotonics.

Acknowledgments TS expresser her sincere gratitude to the financial support of the Council of Scientific and Industrial Research (CSIR), New Delhi in the form of NET-SRF under sanction number 31/015(0060)/2007-EMR-1. They gratefully thank Dr. H. S. Maiti, Director of the institute for kind permission to publish this paper. The technical supports provided by the infrastructural facility of this institute and Unit of Nano Sci. and Nano Tech. (IACS, Kolkata) for TEM experiment are also thankfully acknowledged.

References

1. Schwartzberg AM, Zhang JZ (2008) Novel optical properties and emerging applications of metal nanostructures. J Phys Chem C 112(28):10323–10337
2. Lu X, Rycenga M, Skrabalak SE, Wiley B, Xia Y (2009) Chemical synthesis of novel plasmonic nanoparticles. Ann Rev Phys Chem 60:167–192
3. Prasad PN (2004) Nanophotonics. Wiley, New Jersey, pp 129–151
4. Zhang JZ, Noguez C (2008) Plasmonic optical properties and applications of metal nanostructures. Plasmonics 3(4):127–150
5. Kreibig U, Vollmer M (1995) Optical properties of metal clusters. Springer, Berlin
6. Barnes WL, Dereux A, Ebbesen TW (2003) Surface plasmon subwavelength optics. Nature 424(7):824–830
7. Le F, Brandl DW, Urzhumov YA, Wang H, Kundu J, Halas NJ, Aizpurua J, Nordlander P (2008) Metallic nanoparticle arrays: a common substrate for both surface-enhanced raman scattering and surface-enhanced infrared absorption. ACS Nano 2(4):707–718
8. Murray WA, Barnes WL (2007) Plasmonic materials. Adv Mater 19(22):3771–3782
9. Gonella F, Mazzoldi P (2000) Metal nanocluster composite glasses, in Handbook of Nanostructured Materials and Nanotechnology, Nalwa HS (Ed), vol 4. Academic, San Diego
10. de Lamaestre RE, Béa H, Bernas H, Belloni J, Marignier JL (2007) Irradiation-induced Ag nanocluster nucleation in silicate glasses: Analogy with photography. Phys Rev B 76(20):205431 [18 pages]
11. Blondeau JP, Catan F, Andreazza-Vignolle C, Sbai N (2008) Plasmon resonance and clustering of silver nanoclusters embedded in glass. Plasmonics 3(2–3):65–71
12. Dmitruk I, Blonskiy I, Pavlov I, Yeshchenko O, Alexeenko A, Dmytruk A, Korenyuk P, Kadan V (2009) Surface plasmon as a probe of local field enhancement. Plasmonics 4(2):115–119
13. Zhang AY, Suetsugu T, Kadono K (2007) Incorporation of silver into soda-lime silicate glass by a classical staining process. J Non-Cryst Solids 353:44–50
14. Chen S, Akai T, Kadono K, Yazawa T (2001) A silver-containing halogen-free inorganic photochromic glass. Chem Commun 20:2090–2091
15. Shin J, Jang K, Lim K-S, Sohn I-B, Noh Y-C, Lee J (2008) Formation and control of Au and Ag nanoparticles inside borate glasses using femtosecond laser and heat treatment. Appl Phys A 93(4):923–927
16. Speranza G, Minati L, Chiasera A, Ferrari M, Righini GC, Ischia G (2009) Quantum confinement and matrix effects in silver-exchanged soda lime glasses. J Phys Chem C 113 (11):4445–4450
17. Shin J, Jang K, Lim K-S, Kim Y-S, Lee Y-L, Choi J-H, Sohn I-B, Lee J, Lee M (2009) Formation and removal of multi-layered fluorescence patterns in gold-ion doped glass. Appl Surf Sci 255 (24):9754–9757
18. Yeshchenko OA, Dmitruk IM, Dmytruk AM, Alexeenko AA (2007) Influence of annealing conditions on size and optical properties of copper nanoparticles embedded in silica matrix. Mater Sci Engg B 137(1–3):247–254

19. Hofmeister H, Drost W-G, Berger A (1999) Oriented prolate silver particles in glass-characteristics of novel dichroic polarizers. Nanostruct Mater 12(1–4):207–210
20. Seifert G, Kaempfe M, Berg K-J, Graener H (2000) Femtosecond pump-probe investigation of ultrafast silver nanoparticle defortmation in a glass matrix. Appl Phys B 71 (6):795–800
21. Kassab LRP, de Araújo CB, Kobayashi RA, de Pinto RA, da Silva DM (2007) Influence of silver nanoparticles in the luminescence efficiency of Pr^{3+}-doped tellurite glasses. J Appl Phys 102 (10):103515, 1-4
22. Som T, Karmakar B (2009) Nanosilver enhanced upconversion fluorescence of erbium ions in Er^{3+}:Ag-antimony glass nanocomposites. J Appl Phys 105(1):013102
23. Som T, Karmakar B (2009) Enhancement of Er^{3+} upconverted luminescence in Er^{3+}:Au-antimony glass dichroic nanocomposites containing hexagonal Au particles. J Opt Soc Am B 26(12):B21–B27
24. Pompa PP, Martiradonna L, Della Torre A, Della Sala F, Manna L, De Vittorio M, Calabi F, Cingolani R, Rinaldi R (2006) Metal-enhanced fluorescence of colloidal nanocrystals with nanoscale control. Nature Nanotechnol 1(2):126–130
25. Som T, Karmakar B (2009) Structure and properties of low phonon antimony glasses in the K_2O-B_2O_3-Sb_2O_3-ZnO system. J Am Ceram Soc 93(10):2230–2236
26. Som T, Karmakar B (2008) Infrared-to-red upconversion luminescence in samarium-doped antimony glasses. J Lumin 128(12):1989–1996
27. Som T, Karmakar B (2008) Core-shell Au-Ag nanoparticles in dielectric nanocomposites with plasmon-enhanced fluorescence: a new paradigm in antimony glasses. Nano Res 2:607–616
28. CRC Handbook of Chemistry and Physics (1975) 75th edn, pp.8-21-34. Edited by D. R. Lide. CRC press. Boca Raton
29. Terashima K, Hashimoto T, Uchino T, Kim S-H, Yoko T (1996) Structure and nonlinear optical properties of Sb_2O_3-B_2O_3 binary glasses. J Ceram Soc Jpn 104(11):1008–1014
30. Nalin M, Messaddeq Y, Ribeiro SJL, Poulain M, Briois V, Brunlkaus G, Rosenhahn C, Mosel BD (2004) Structural organization and thermal properties of the Sb_2O_3–$SbPO_4$ glass system. J Mater Chem 14(23):3398–3405
31. Beall GH, Duke DA (1983) Glass Ceramic Technology, in Glass: Science and Technology, Uhlman DR, Kreidl NJ (Eds.), vol 1, Academic Press, San Diego.
32. Fort E, Ricolleau C, Sau-pueyo J (2003) Dichroic thin films of silver nanoparticle chain arrays on facetted alumina templates. Nano Lett 3(1):65–67
33. Dirix Y, Bastiaansen C, Caseri W, Smith P (1999) Oriented pearl-necklace arrays of metallic nanoparticles in polymers: a new route toward polarization-dependent color filters. Adv Mater 11(3):223–227
34. Link S, El-Sayed MA (1999) Spectral properties and relaxation dynamics of surface plasmon electronic oscillations in gold and silver nanodots and nanorods. J Phys Chem B 103(40):8410–8426
35. Stephan L, El-Sayed MA (1999) Size and temperature dependence of the plasmon absorption of colloidal gold nanoparticles. J Phys Chem B 103(21):4212–4217
36. Kelly KL, Coronado E, Zhao LL, Schatz GC (2003) The optical properties of metal nanoparticles: The influence of size, shape and dielectric environment. J Phys Chem B 107(3):668–677
37. Schmid G (2008) General Features of Metal Nanoparticles Physics and Chemistry, in Metal Nanoclusters in catalysis and materials science: The issue of size control, Corain B, Schmid G, Toshima N (Eds.), Elsevier, Amsterdam, pp. 3–20.
38. Pérez-Juste J, Pastoriza-Santos I, Liz-Marzán LM, Mulvaney P (2005) Gold nanorods: synthesis, characterization and applications. Chem Coord Rev 249(17–18):1870–1901
39. Myroshnychenko V, Rodríguez-Fernández J, Pastoriza-Santos I, Funston AM, Novo C, Mulvaney P, Liz-Marzán LM, de Abajo FJG (2008) Modelling the optical response of gold nanoparticles. Chem Soc Rev 37(9):1792–1805
40. Lakowicz JR, Malicka J, Gryczynski I, Gryczynski Z, Geddes CD (2003) Radiative decay engineering: the role of photonic mode density in biotechnology. J Phys D Appl Phys 36(14):R240–R249
41. Hayakawa T, Selvan ST, Nogami M (1999) Field enhancement effect of small Ag particles on the fluorescence from Eu^{3+}-doped SiO_2 glass. Appl Phys Lett 74(11):1513
42. Matveeva EG, Shtoyko T, Gryczynski I, Akopova I, Gryczynski Z (2008) Fluorescence quenching/enhancement surface assays: signal manipulation using silver-coated gold nanoparticles. Chem Phys Lett 454(1–3):85–90
43. Geddes CD, Gryczynski I, Malicka J, Gryczynski Z, Lakowicz JR (2003) Metal-enhanced fluorescence: potential applications in HTS. Comb Chem High Through Screen 6(2):109–117
44. Stranik O, Nooney R, McDonagh C, MacCraith BD (2007) Optimization of nanoparticle size for plasmonic enhancement of fluorescence. Plasmonics 2(1):15–22